Microwave Reflection Tomography Array for Damage Detection in Concrete Structures

Yoo Jin Kim[1], Luis Jofre[2], Franco De Flaviis[1], and Maria Q. Feng[1]

[1]University of California, Irvine, CA 92697, USA
[2]Technical University of Catalonia, Barcelona, Spain

Abstract — **Microwave sub-surface imaging system for structural damage detection using reflection array is developed. The analytical expressions of bi-focusing procedures are derived and applied to a series of numerical simulations. Slot antenna array is designed and fabricated for experimental study. From the results of measurements, it is demonstrated that the proposed imaging system can reconstruct sub-surface images efficiently.**

I. INTRODUCTION

Nondestructive assessment of concrete structures, currently, heavily relies on visual inspections, which apparently have some limitations. Majority of highway bridges are concrete bridges, and such invisible damage as voids and cracks inside concrete and debonding between rebars and concrete caused by corrosions and earthquakes is of significant concern.

In this study, extending preliminary experimental and analytical works [1-2], a microwave sub-surface imaging system using cylindrical array is developed and verified for its capabilities to assess damages inside concrete structures. The proposed sub-surface imaging system proposed uses an arrangement consisting of several cylindrical/planar arrayed antennas for transmitting and receiving signals, and a numerical focusing operator is applied to the external signals both in transmitting and in receiving fields.

This paper describes the capabilities of microwave sub-surface imaging system for structural damage detection using reflection arrays. First, a numerical focusing procedure, which allows the recovery of a 2-dimensional object from its scattered field, is described. Second, some numerical simulations for the study of reconstruction parameters and the verification of reconstruction algorithm are presented. Finally, experimental verifications through the tests on the concrete blocks demonstrated that the sub-surface focused imaging system using the proposed antenna array can successfully detect the voids and defects inside the concrete structure.

II. ANALYTICAL FORMULATION AND RECONSTRUCTION PARAMETERS

A. Analytical Formulation

The measurement geometry, shown in Fig. 1, uses $N_n \times N_m$ elements, N_n forming a cylindrical transmitting array and N_m forming a cylindrical receiving array. A $N_n \times N_m$ measurement matrix can be obtained as follows: for every selected transmitting element, the receiving array is scanned obtaining an N_m-measurement column, then the procedure is repeated for the N_n elements of the transmitting array.

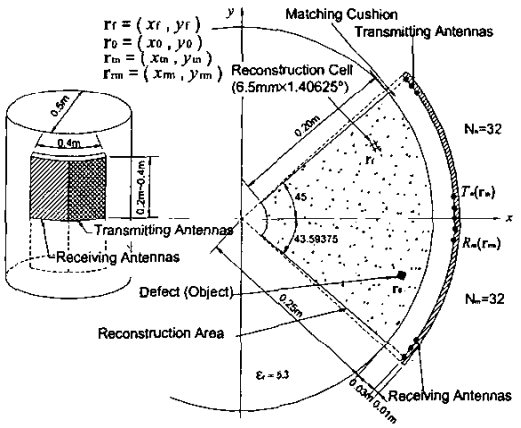

Fig. 1. Measurement geometry for two cylindrical transmitting and receiving arrays of 32 elements.

Following the electromagnetic compensation principle, the illumination of an object induces an equivalent electric current distribution, $J_{eq}(x_0,y_0,z_0)$, and this distribution makes electromagnetic image of interest in recovering [3]. The reconstruction algorithm forms every image point by means of the synthesis of two focused arrays (transmitting and receiving arrays), i.e. all the elements of both arrays are weighted by focusing operator so as to be focused on a unique object point. This can be achieved by numerical treatment of the measurement matrix.

0-7803-7239-5/02/$10.00 © 2002 IEEE

The focusing operator can be obtained by taking an inverse of the field induced by a current line. It is well known that the electric fields of the infinite electric line source is proportional to a Hankel function of the second kind whose argument is proportional to the distance from the source to the observation point. Therefore, the incident field at $\mathbf{r}_i(x_i,y_i)$ when focusing on every transmitting point $\mathbf{r}_{tn}(x_{tn},y_{tn})$ on the reconstructing point $\mathbf{r}_f(x_f,y_f)$ can be expressed as

$$E_i(x_i,y_i)=\sum_{n=1}^{N_t} I_{Tn}(x_f,y_f)\cdot H_0^{(2)}(k_e\,|\,\mathbf{r}_{tn}-\mathbf{r}_i\,|) \quad (1)$$

where $I_{Tn}(x_f,y_f)$, focusing operator, is given by

$$I_{Tn}(x_f,y_f)=\frac{1}{H_0^{(2)}(k_e\,|\,\mathbf{r}_{tn}-\mathbf{r}_f\,|)} \quad (2)$$

and k_e is wavenumber in concrete (ε_r=5.3).

Scattered field measured at $\mathbf{r}_{rm}(x_{rm},y_{rm})$ of a defect (object) placed at $\mathbf{r}_0(x_0,y_0)$ is

$$E_s(x_{rm},y_{rm})=E_i(x_0,y_0)\cdot I_{obj}\cdot H_0^{(2)}(k_e\,|\,\mathbf{r}_{rm}-\mathbf{r}_0\,|) \quad (1)$$

where I_{obj} is a constant for every object containing its electromagnetic macroscopic characteristics.

When focusing back the received field at $\mathbf{r}_{rm}(x_{rm},y_{rm})$ on the interest point $\mathbf{r}_f(x_f,y_f)$, electromagnetic image of $E_f(x_f,y_f)$ at $\mathbf{r}_f(x_f,y_f)$ can be expressed as

$$E_f(x_f,y_f)=\sum_{m=1}^{N_r} E_s(x_{rm},y_{rm})\cdot I_{Rm}(x_f,y_f) \quad (4)$$

where $I_{Rm}(x_f,y_f)$, focusing operator, is given by

$$I_{Rm}(x_f,y_f)=\frac{1}{H_0^{(2)}(k_e\,|\,\mathbf{r}_{rm}-\mathbf{r}_f\,|)} \quad (5)$$

Finally, all the process can be grouped as follows:

$$E_f(x_f,y_f)=\begin{bmatrix} I_{T1} & I_{T2} & \cdots & I_{Tn}\end{bmatrix}\cdot\begin{bmatrix} E_{s,T1R1} & E_{s,T1R2} & \cdots & E_{s,T1Rm}\\ E_{s,T2R1} & E_{s,T2R2} & \cdots & E_{s,T2Rm}\\ \vdots & \vdots & \ddots & \vdots\\ E_{s,TnR1} & E_{s,TnR2} & \cdots & E_{s,TnRm}\end{bmatrix}\cdot\begin{bmatrix} I_{R1}\\ I_{R2}\\ \vdots\\ I_{Rm}\end{bmatrix} \quad (6)$$

B. Reconstruction Parameters

The formulation derived in the previous section has been applied to the case of two cylindrical arrays of 32 antennas each, with frequency of 10 GHz (λ_0= 3.0 cm, λ_e= 1.3 cm). In order to study the focusing capability of the system at different distances of the array and view angles, nine point-like objects were placed at boundary and central landmark points of the reconstructing 2D cross section. The results, as shown in Fig. 2(a), show a good uniformity of the 9 point focusing intensity level and impulse response shape that suggest a very good behavior of the reconstruction algorithm.

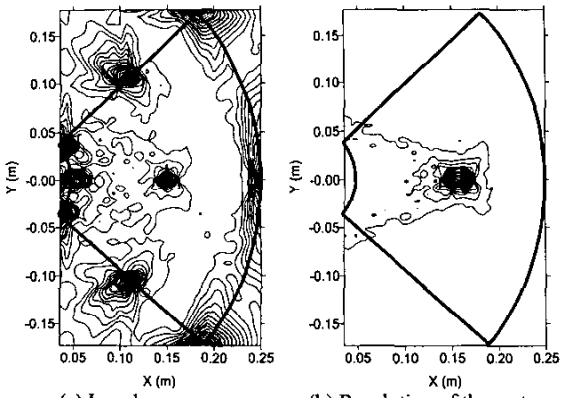

(a) Impulse response (b) Resolution of the system

Fig. 2. Reconstruction parameters of the system.

In addition, simulations using numerical measurements have been conducted in order to verify the resolution capabilities of the system. The results, as shown in Fig. 2(b), demonstrate that the system, due to the use of bi-focusing (focusing both the transmitting and receiving arrays), is able to achieve a resolution in the order of the wavelength in the dielectric medium (1.3cm). This clearly improves the resolution of a conventional system using mono-focusing (focusing the receiving array only) [4].

III. REFLECTION TOMOGRAPHIC ARRAY

A planar rectangular microwave antenna is designed at 5.2 GHz as an illuminating frequency, which has been chosen as a reasonable tradeoff between attenuation and resolution, based on the electrical and geometrical parameters of the different sizes of structures to be inspected. As shown in Fig. 3, the planar rectangular microwave antenna is composed of two rectangular halves, composed of 8 × 8 slot antenna array each, acting as transmitting and receiving antennas respectively. Each one of these two planar 8 × 8 arrays consists of a parallel fed 8-element vertical array producing a tomographic focused slice perpendicular to the axis of the column, and an electronically switched 8-element horizontal array able to focus a particular point inside the previous horizontal focused slice. The first array, the transmitting antenna, focuses the illuminating fields on a particular point inside the volume of investigation and the

second one focuses the receiving beam on the same previous point. The whole antenna is a sandwich structure with two metallic grounded substrates separated by a light foam layer. The grounded substrate close to the column contains the radiating $\lambda/2$ slots in the exterior ground plane and the 100 Ω microstrip feeding line on the interior side. The second grounded plane, $\lambda/4$ apart from the slot plane, acts as a reflector in order to produce a unidirectional radiation towards the volume of investigation. Example of S_{ii} parameters measurement is plotted in Fig. 4.

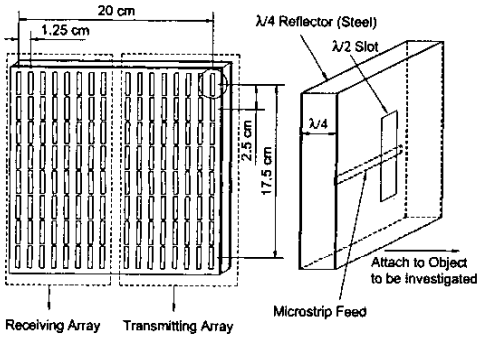

Fig. 3. Planar rectangular microwave antenna array.

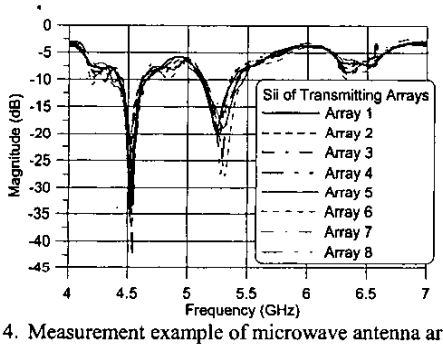

Fig. 4. Measurement example of microwave antenna array.

IV. Experimental Verification

A. Experimental Setup and Calibration

The effectiveness of the proposed sub-surface imaging technology using microwave antenna array is investigated through a series of experiments on a concrete block.

A rectangular concrete block having dimension of 30cm×30cm×30cm is prepared for experimental study. Two types of artificial voids are generated inside of concrete block; one is square Styrofoam block of 2cm on the side and the other one is rectangular Styrofoam bar of 5cm×2cm×2cm. Each of them is inserted into the concrete during the pouring of concrete with the distance of 3 cm from the face of concrete to the face of Styrofoam in both cases.

Experimental setup consists of network analyzer, switch box, coaxial cables and antenna array as represented in Fig. 5. The network analyzer is used to evaluate the transmitted portion of signal through the medium (S_{12}). The switch box is a RF network capable of controlling multiple antennas in the array and selecting them individually to perform S_{12} measurement.

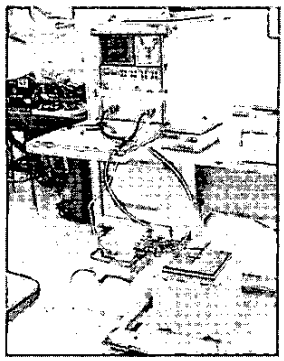

Fig. 5. Experimental setup.

In order to remove the effect of wave reflections and loss in the coaxial cables and/or in the switch box from the measurement matrix, calibration with respect to each transmission measurement ($S_{ij}^{(mea)}$) was needed. For the calibration purpose, concrete panel without defect and steel plate were used.

Each transmission measurement without all the effects from the coaxial cables and the switch box, which is from the transmitting array to the receiving one, is proportional to the zero-order Hankel function of the second kind, $H_0^{(2)}(k_{e,conc}\, d_{ij})$, whose argument is proportional to the distance from the transmitting array to the receiving one, d_{ij} [5]. All the measurement effects from the coaxial cables and the switch box (calibration factor), therefore, can be calculated by dividing each transmission measurement of calibration ($S_{ij}^{(cal\_mea)}$) by the zero-order Hankel function of the second kind, and the calibrated transmission measurement ($S_{ij}^{(cal)}$) can be obtained by dividing each transmission measurement ($S_{ij}^{(mea)}$) by calibration factor, as follows for the case of transmitting array i and receiving array j.

$$S_{ij}^{(cal)} = \frac{S_{ij}^{(mea)}}{Cal\_Factor} \tag{7}$$

where

$$Cal\_factor = \frac{S_{ij}^{(cal\_mea)}}{H_0^{(2)}(k_{e,conc} d_{ij})} \tag{8}$$

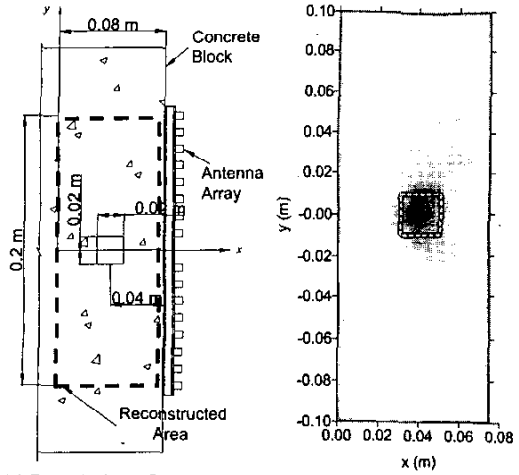

(a) Description of case 1 (b) Reconstructed image

Fig. 6. Experimental result of case 1.

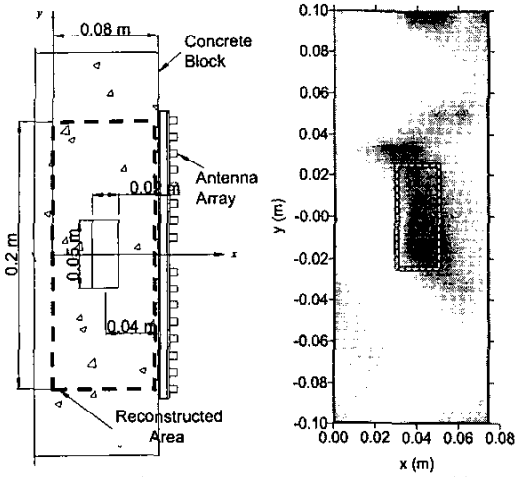

(a) Description of case 2 (b) Reconstructed image

Fig. 7. Experimental result of case 2.

The calibration factors of each transmission measurement at 5.2 GHz were used for calculating the calibrated measurement matrix.

B. Experimental Results

Continuous sinusoidal EM wave with its frequency sweeping from 4.0 GHz to 7.0 GHz, same frequency range used in antenna design, were generated from the signal analyzer and sent to the test specimen. Switch box controls the location of transmitting and receiving arrays from $S_{1,9}$ to $S_{8,16}$. Transmission measurements of each transmitting and receiving array pair at 5.2 GHz were assembled into measurement matrix.

Each measured signal was divided by calibration factor at 5.2 GHz as described in previous section, and was assembled into calibrated measurement matrix to be multiplied by numerical focusing operators. The reconstructed images of center cut in each case are plotted in Fig. 6 and Fig. 7 by the amplitude of electric current distributions.

Two-dimensional descriptions are illustrated in Fig. 6(a) and Fig. 7(a). The results from both cases show that the images of square and rectangular Styrofoam's are successfully reconstructed in terms of size and location, as represented in Fig. 6(b) and Fig. 7(b).

V. CONCLUSIONS

A sub-surface focused microwave imaging technology has been developed in this study for detecting damages or objects inside of concrete structures. The following conclusions are be drawn from simulation analysis and experiments:

(1) The simulation results show that the reconstruction algorithm gives a uniformity of focusing intensity level and the resolution can be improved by focusing both in transmitting and receiving arrays.

(2) A slot antenna array working in front of a dielectric medium is designed and fabricated. The performance of the antenna array is tested and verified that the slot antenna array is appropriate to use for damage detection for concrete structures in terms of its radiation performance and bandwidth.

(3) From the results of experiments with concrete specimen, the air void can be successfully detected in terms of the location and the size.

REFERENCES

[1] M. Q. Feng, F. D. Flaviis, and Y. J. Kim, "Use of Microwaves for Damage Detection of FRP-Wrapped Concrete Structures" *Journal of Engineering Mechanics, ASCE*, Vol.128, No.2, pp.172~183, 2002.

[2] Y. J. Kim, L. Jofre, F. De Flaviis, and M. Q. Feng, "Microwave Cylindrical Reflection Imaging Array For Structural Damage Detection", *Proceedings of IEEE AP-S/URSI Symposium*, pp.678~681, Boston, MA, 2001.

[3] I. M. Girones, L. Jofre, M. Ferrando, M. De Los Reyes, and J. C. Bolomey, "Microwave Imaging with Crossed Linear Arrays", *IEE Proceedings*, Vol.134, Pt. H, No.3, June, 1987.

[4] S. X. Pan and A. C. Kak, "A Computational Study of Reconstruction Algorithms for Diffraction Tomography: Interpolation vs. Filtered-Backpropagation", *IEEE Trans. Acoust. Speech Signal Processing*, Vol. ASSP-31, pp. 1262~1275, October, 1983.

[5] Contantine A. Balanis, *Advanced Engineering Electromagnetics*, John Wiley & Sons, 1989